Amsterdam '14

Th E106 11

# Full Waveform Inversion on Jackdaw Ocean Bottom Nodes Data in North Sea

K. Yoon (TGS), P. Moghaddam (TGS), I. Vlad (TGS), M. Warner (Imperial College London) & J. Sheng* (TGS)

## SUMMARY

A FWI workflow for Jackdaw Ocean Bottom Node (OBN) dataset is described. Small receiver coverage, large receiver crossline spacing and no well information make it challengeable to apply FWI against this dataset. Improved shallow velocities and increasing offset, depth and traveltime enable us to get high resolution shallow FWI velocity model. Source estimation using near offset direct waves is a good approach for shallow sea bottom data. Convergence of FWI was confirmed by shallow depth slices of velocity model, seismogram comparison and phase residual between observed and synthetic seismograms.

## Introduction

This is a case study of the application of Full Waveform Inversion (FWI) to an Ocean Bottom Node (OBN) Jackdaw dataset in North Sea. The workflow followed to acquire a promising shallow velocity resolution is described in a step-by-step manner. Many factors affect the results of FWI. Properties such as initial model, data acquisition type, preprocessing, source wavelet and inversion algorithm are critical to FWI results. Therefore it is important to determine an effective workflow for each dataset. Recently, Warner et al. (2013) and Bansal et al. (2013) improved velocity models using anisotropic FWI with OBN data. We applied FWI to a challenging OBN dataset. Receivers covering 6% of the survey are located with 500 m crossline spacing. Shallow velocities were difficult to be defined well due to large receiver spacing, small receiver coverage and lack of well information. Routine FWIs starting from traveltime tomography velocity model were not successful. FWI began to converge after improving shallow velocities and gradually increasing offset, depth and traveltime simultaneously. This workflow needs painful manual velocity rebuilding at each offset range. However it can be an effective FWI approach in case the initial velocity model is far from the true velocity model.

## OBN Data

The survey consists of 53900 sources distributed over an area of 243 km$^2$ with 25 m inline and 200 m crossline spacing (Figure 1). There are 6 OBN receiver lines composed of 698 nodes with 50 m inline and 500 m crossline spacing over 15 km$^2$ area in the middle of survey. FWI is an attractive velocity modeling tool where you have full azimuthal coverage and particularly if there are long offsets data, as in this case, of up to 11 km. In this study, we used all 698 OBN receivers and every 5$^{th}$ source. The source decimation and additional 6 ms resampling reduced the original file size from 360 GB to about 40 GB. Source decimation didn't create noticeable footprints in FWI velocity. However, 500 m receiver and 200 m source crossline spacing are too large that these remained footprints on FWI velocities. The depth of sea bottom is about 70 m.

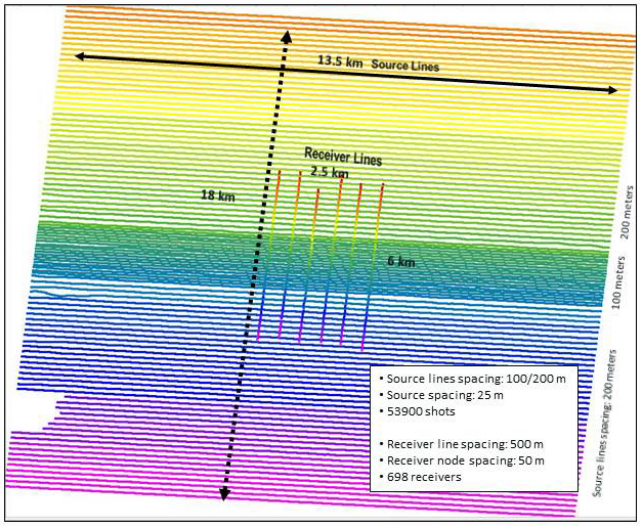


*Figure 1. Acquisition geometry and specifications of Jackdaw OBN data in North Sea. A total of 698 nodes make up 6 receiver lines covering 15 km$^2$ area in the middle of survey. 53900 sources are distributed over the whole survey area of 243 km$^2$.*

## Data preprocessing & source wavelet

In this study, we used hydrophone data including multiples and ghosts. Figure 2(a) is an offset receiver gather filtered by 0 Hz ~ 9 Hz filter. Only early arriving events were preserved by muting for FWI. We started source wavelet estimation by stacking filtered and shifted near offsets of the observed data in Figure 2(a). Near offset traces were aligned using a water velocity of 1498 m/sec before stacking. Because the wavelet estimated by the stack of low pass near offset seismograms is not causal, the filtered observed data was shifted down by 500 ms for causal source wavelet and FWI. Least squares FWI, which we used in this study, updates parameters so that the synthetic data improves the match to the observed data. Near offsets preserve original source wavelet most likely. No matter what kind of physics we implement in wave propagation, the source wavelet is acceptable only if near offset synthetic seismograms fit the observed data well. We used isotropic acoustic wave equation with free surface boundary and didn't apply deghosting and demultiple. In shallow sea bottom data, low pass filtering makes direct wave, sea bottom reflection, shallow reflections and multiples to mingle in near offsets. Source wavelet of low pass filtered seismogram is different from the low pass filtered acquisition airgun source wavelet. Therefore, we decided to determine the source wavelet from near offsets of observed data directly rather than filter the high-frequency acquisition

wavelet after deghosting and demultiple. We stacked the traces over 100 m ~ 300 m offset in Figure 2(a) to make initial source wavelet $S_0$ shown in Figure 3(a). Synthetic seismogram $U$ was generated using the initial source wavelet $S_0$. New source wavelet $S_{new}$ was updated from the initial source wavelet $S_0$, observed data $D$ and synthetic data $U$ following the source estimation method:

$$S_{new} = S_0(\sum D^* U / \sum UU^*) \quad (1)$$

as described by Pratt (1999) in frequency domain. Then new synthetic seismogram $U_{new}$ was generated from $S_{new}$. The final source wavelet shown in Figure 3(b) was obtained by shifting $S_{new}$ by the maximum cross correlation delay between synthetic seismogram $U_{new}$ and observed data $D$. Figure 2(b) and 2(c) are synthetic seismograms generated from the final source wavelet using initial and FWI velocity models, respectively. Figure 3(c), (d) and (e), which are enlarged near offset traces of Figure 2(a), 2(b) and 2(c), show that our final source wavelet is acceptable. In Figure 2(b) and 3(d), synthetic seismograms from initial velocity model fit observed data at very near offsets only. However, in Figure 2(c) and Figure 3(e), synthetic seismograms after FWI match the observed data well over whole offset.

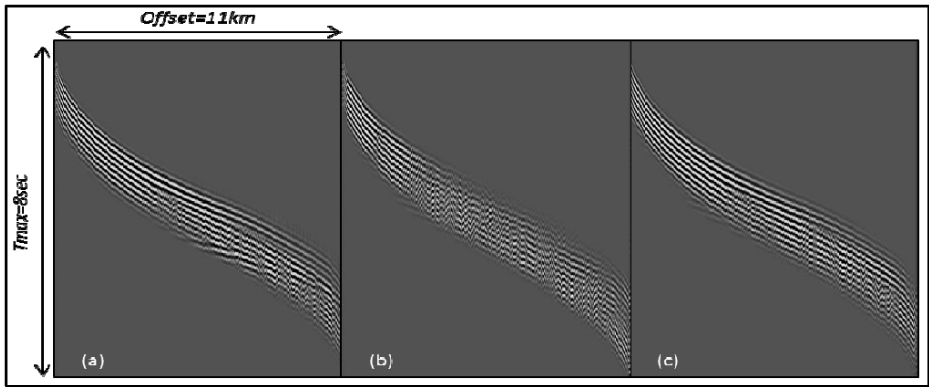


*Figure 2. (a) an observed receiver offset gather after low pass filter, muting and 500 ms shift down. Synthetic seismograms from final source wavelet and (b) initial and (c) FWI velocity models.*

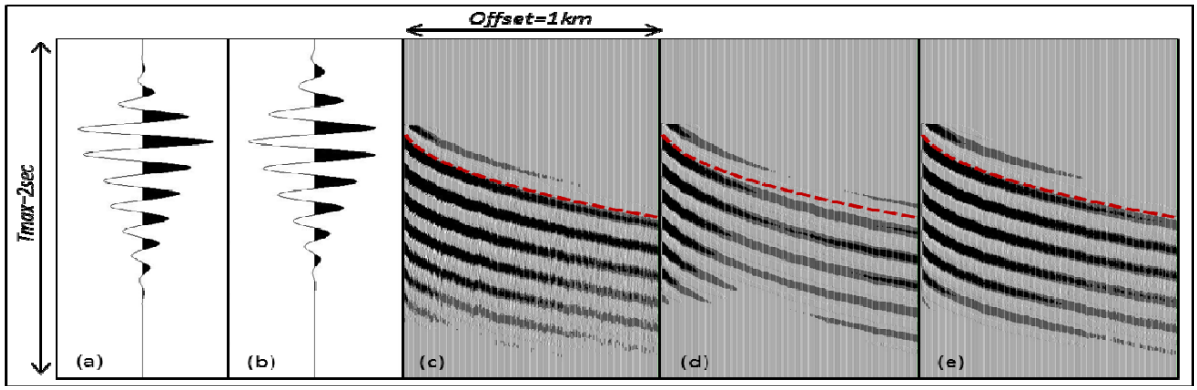


*Figure 3. (a) initial source wavelet obtained by near offset traces stacking and (b) final updated and shifted source wavelet. Near offsets in (c) observed data and synthetic seismograms using (d) initial and (e) FWI velocity models. The red dash lines in Figure 3(c), 3(d) and (3e) are same traveltime curves picked from 3(c).*

**Initial velocity model**

Good initial velocity model is critical for successful FWI. Receivers of Jackdaw dataset are distributed at the middle of survey over 6% of whole area. We started from traveltime tomography within the area covered by receivers. Velocities outside of receivers were filled out by extrapolation of the velocities below receivers. Figure 4(a) is the initial velocity model after extrapolation and smoothing. The initial velocity model is too simple to believe it is close to the true velocity. Figure 2(b) and Figure 3(d), synthetic seismograms generated from the initial velocity model, show poor matching to the observed data and significant traveltime errors within 1 km offset as denoted by red dash line in Figure 3(d). The traveltime error indicates that initial velocities are too low at shallow

depth. 500 m receiver crossline spacing made it difficult to obtain correct shallow velocities. However, we could get an effective workflow for FWI starting from ill-defined initial velocity model through this study.

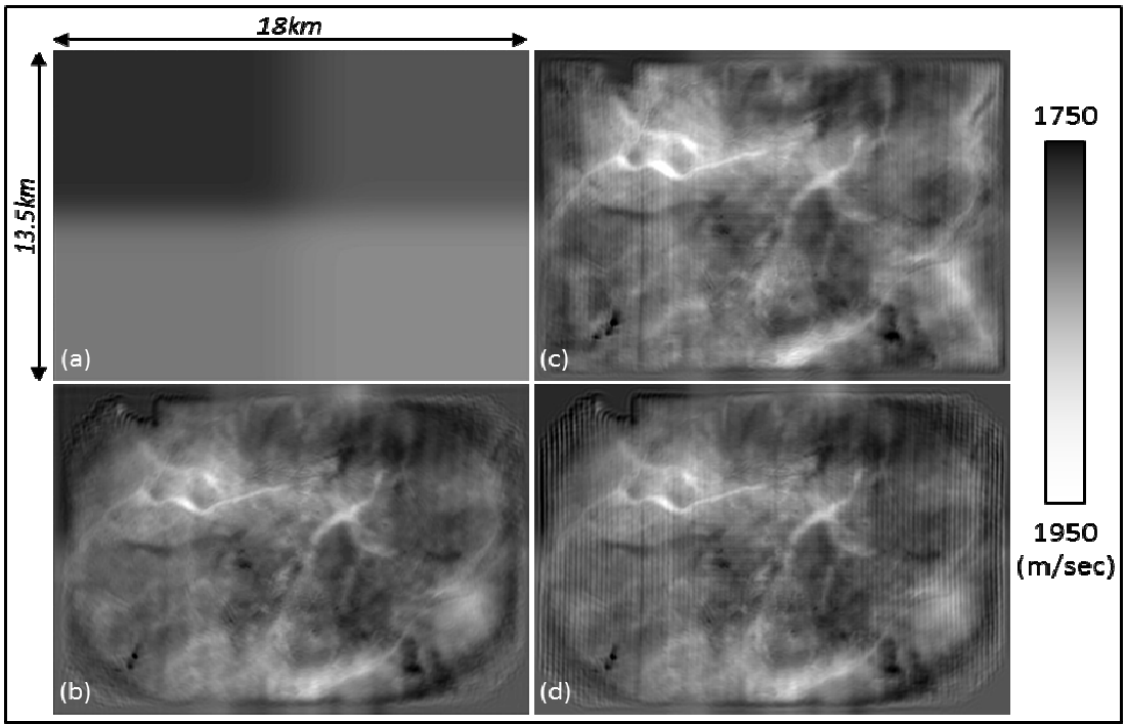


*Figure 4. Velocity slices at 240 m depth; (a) initial velocity, (b) FWI velocity after foot print removal at 0 ~ 7 km offset, FWI velocities without footprint removal at (c) 0 ~ 11 km and (d) 0 ~ 7 km offsets.*

**Inversion**

We used isotropic wave equation with free surface boundary and 40 m cubic grid for wave propagation modelling. Each trace in observed and synthetic data has been normalized for phase only inversion. The sizes of velocity are 18 km, 13.5 km and 3 km in inline, crossline and depth directions. Several tests starting from the initial mode in Figure 4(a) and using whole offset and mid offsets of 0~4 km and 0~7 km had failed. QC tools such as seismogram comparison, phase residual plot (Shah et al., 2012) and gather flatness had convinced the failures. Because, Figure 3(d), the synthetic seismogram from the initial velocity, shows significant traveltime error at 1 km offset already, we updated shallow velocities by FWI with 0~2 km offset, 500 m depth and 2 second traveltime constraints. Then a new initial velocity was built by extrapolation and smoothing. Starting from the new initial velocity model, we performed multiple FWIs by increasing offset by 1 km from 0~1 km to 0~11 km. Maximum depth and traveltime were increased simultaneously according to the offset increment. After FWI at each offset range, FWI velocity model was smoothed mildly with 200 m radius and the central velocities were extrapolated to the boundaries. The smoothed and extended velocity model was used as the initial velocity model for the next offset FWI.
FWI gradient has edge effects at the end of offset and maximum penetrating depth of turning wave. Velocity extrapolation from the central area and increment of maximum depth of velocity update are effective to avoid edge effects. By improving shallow depth in initial velocity and opening offset, depth and traveltime simultaneously, FWI began to converge and QC tools confirmed the convergence. Figure 5 shows the FWI velocities at 7 km offset, which used (a) the initial velocity model and (b) 6 km offset FWI velocity model started from the improved initial velocity model as FWI starting models. FWI started from the initial model produced severe edge effects and footprints. However, these noises reduced in FWI using 6 km offset FWI velocity model as the starting model.
Figure 4(b) and 4(d) are velocity slices at 240 m depth at 0~7 km offset after and before footprint removal. Large receiver and shot line spacing created horizontal receiver and vertical shot footprints.

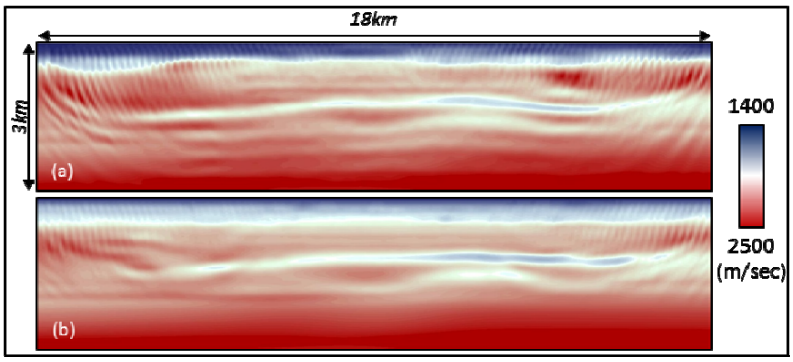


*Figure 5. FWI velocities at 7 km offset range, which used (a) the initial velocity model and (b) 6 km offset FWI model started from the improved initial model as the starting velocities. Please note the severe edge effects and footprints in (a), which reduced in conver-ging FWI in (b).*

Footprints can be eliminated by $K_x$-$K_y$ filtering as shown in Figure 4(b). Figure 4(c) is the velocity model without footprint removal at 0~11 km offset FWI. In Figure 4(c), velocities are defined well over whole survey and footprints are less severe than velocity of smaller offset range in Figure 4(d). Correct velocities seem to reduce footprints. Visual comparison to the seismograms is the most straightforward QC tool. Figure 2(c), synthetic seismogram after FWI, matches the observed data in Figure 2(a) well. Figure 6 display vertical slices of velocities and Reverse Time Migrations (RTM) up to 1 km depth along a line parallel to the receiver lines. Figure 6(e), RTM using FWI velocity model, shows enhanced image. In Figure 6(c), FWI velocity update indicates velocity increment around 100 m ~ 300 m depth, which we expected from the traveltime error in Figure 3(e).

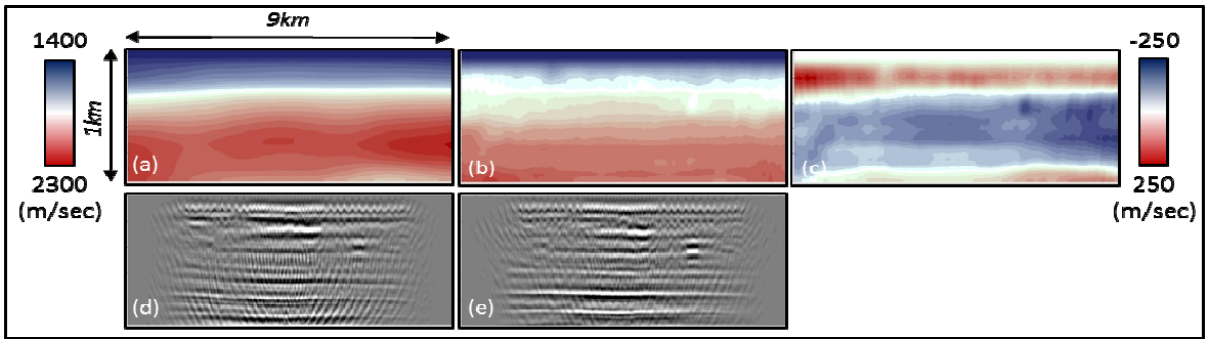


*Figure 6. Vertical velocity sections (a) before and (b) after FWI. (c) velocity update by FWI. RTMs (d) before and (e) after FWI.*

## Conclusions

We produced a high-resolution shallow velocity on an OBN dataset with large receiver and source crossline spacing and ill-defined initial velocity model. In case the initial velocity is far from the true velocity, the shallow depth needs to be defined well first and a gradual opening offset, depth and time is an effective workflow. Source wavelet estimation from near offsets stacking and shifting for phase matching is a good approach for shallow sea bottom data.

## References

Bansal, R., Routh, P., Krebs, J., Lee, S., Baumstein, A., Anderson, J., Downey, N., Lazaratos, S., Lu, and Saldarriaga, R., 2013, Full wavefield inversion of ocean bottom node data: 75th Conference and Exhibition, EAGE, Extended Abstracts, WE1104.

Pratt, R. G., 1999, Seismic waveform inversion in the frequency domain, Part I: Theory and verification in a physical scale method: Geophysics, **64**, 888-901, http://dx.doi.org/10.1190/1.1444597.

Shah, N., Warner, M., Nangoo, T., Umpleby, A., Stekl, I., Morgan, J. and Guasch, L., 2012, Quality assured full-waveform inversion: Ensuring starting model adequacy, 82nd Annual International Meeting, SEG, Expanded Abstracts, SI3.5, http://dx.doi.org/10.1190/segam2012-1228.1.

Warner, M., Ratcliffe, A., Nangoo, T., Morgan, J., Umpleby, A., Shah, H., Stekl, I., Guasch, L., Win, C., Conroy, G., and Bertrand, A., 2013, Anisotropic 3D full-waveform inversion: Geophysics, **78**, no. 2, R59-R80, http://dx.doi.org/10.1190/geo2012-0338.1.